JVST A
Journal of Vacuum Science & Technology A
ARTICLE
pubs.aip.org/avs/jva

Consequences of pulsing low frequency biases in inductively coupled plasmas on ion energy distributions for high aspect ratio plasma etching

Cite as: J. Vac. Sci. Technol. A **44**, 043003 (2026); doi: 10.1116/6.0005333
Submitted: 19 January 2026 · Accepted: 26 May 2026 ·
Published Online: 12 June 2026

Evan Litch,[1,a)] Hyunjae Lee,[2,a)] Sang Ki Nam,[3] and Mark J. Kushner[4,a)]

AFFILIATIONS

[1]Nuclear Engineering and Radiological Sciences Department, University of Michigan, 2355 Bonisteel Blvd, Ann Arbor, Michigan 48109
[2]Memory Manufacturing Technology Center, Samsung Electronics Co., Ltd., 1-1 Samsungjeonja-ro, Hwaseong-si, Gyeonggi-do 18448, South Korea
[3]Samsung Electronics Co., Ltd., 1-1 Samsungjeonja-ro, Hwaseong-si, Gyeonggi-do 18448, South Korea
[4]Electrical Engineering and Computer Science Department, University of Michigan, 1301 Beal Ave., Ann Arbor, Michigan 48109-2122

[a)]**Authors to whom correspondence should be addressed:** elitch@umich.edu; hj0928.lee@samsung.com; and mjkush@umich.edu

ABSTRACT

With the increase in aspect ratio of features in microelectronics fabrication, the trend in plasma etching of high aspect ratio features is toward the use of very low frequencies (VLFs) for substrate biases. With substrate biases of 100s kHz, the maximum ion energy onto the wafer generally increases for a given voltage amplitude. Industry trends are also toward pulsing the substrate bias to control the neutral to ion flux ratios onto the wafer. A consequence of pulsing with VLF is that the DC self-bias on the blocking capacitor, V_{DC}, becomes dynamic. Depending on the RC time constant for charging and discharging V_{DC} relative to the bias-on and bias-off portions of the pulsed cycle, V_{DC} can significantly vary during the pulse period. These dynamics can then affect the ion energy distributions (IEDs) incident onto the wafer. A computational investigation was conducted on IEDs incident onto the wafer in an inductively coupled plasma sustained in $Ar/Cl_2/O_2$ mixtures with a pulsed substrate bias of 250 kHz. Trends of V_{DC}, peak-maximum-energy (the most probable ion energy onto the wafer), and IEDs during the bias-on and bias-off portions of the cycle are discussed as a function of pulse repetition frequency, duty cycle, blocking capacitance, and the focus ring (FR) electrical properties. IEDs during the bias-off portion of the pulse period are most sensitive to these dynamics in V_{DC}. Pulsing reduced the angular tilt of the IED at the edge of the wafer, a critical consideration for minimizing edge exclusion, when compared with continuous excitation. Pulsing reduced the charging of the FR, which, in turn, reduced the sheath curvature at the edge of the wafer.

I. INTRODUCTION

A focus of semiconductor device manufacturing is to increase device densities by using three-dimensional (3D) stacks to augment the traditional two-dimensional shrinkage.[1,2] The focus on producing stacks of 3D devices emphasizes the importance of high aspect ratio (HAR) etching of conductors and dielectrics.[2] For example, 3D NAND, memory now consists of stacks of several hundred cell layers with forecasts of 500–1000 layers, whose fabrication begins with etching of a HAR via having an aspect ratio (AR) approaching and soon to exceed 100.[3] Deep trench isolation (DTI) is a HAR feature etched in Si used to electrically isolate 3D logic and imaging devices.[4]

Gas mixtures containing halogens (e.g., HBr or Cl_2) are used in reactive ion etching of the conductive silicon substrates for DTI features. A capacitively coupled bias is applied to the substrate accelerating ions into the wafer, which originate from the bulk plasma produced by either capacitive or inductive coupling. For etching HAR features, the ion energy and angular distributions (IEADs) incident onto the wafer should have a narrow angular spread from the vertical while having a critically high energy, in some cases exceeding several keV. These specifications enable an acceptable etch rate as the AR increases while maintaining critical dimensions throughout the feature. A current trend in HAR etching is to increase the bias voltage (>5–10 kV) to increase ion energies and reduce the angular spread of ions incident onto the wafer.[5,6] Since sputtering rates typically scale as the square root of ion energy, increasing etch rate by increasing the bias voltage results in diminishing returns.[7,8]

For a given applied voltage, one strategy to increase ion energy is to operate biases with very low frequencies (VLFs), typically with radio frequencies (RFs) less than 1 MHz, and to place transit of ions across the sheath in the *thin-sheath-limit*.[9,10] In this limit, ions cross the sheath in a small fraction of the RF cycle and so, in the absence of collisions, will arrive at the substrate with an energy corresponding to the instantaneous sheath potential. The maximum ion energies onto the substrate when operating with VLFs nearly reach the maximum allowed, $V_o - V_{DC}$, where V_o is the amplitude of the RF bias and V_{DC} is the DC self-bias, which is usually negative.[11,12] The increase in the maximum energy is also accompanied by a decrease in the minimum energy, extending as low as $V_o + V_{DC}$.

Industrial applications of HAR plasma etching are shifting toward the use of pulsed biases to optimize the ratio of radical to ion fluxes to the wafer and to enable alternating periods of etch and passivation.[13–15] At high AR, ion energies to the etch front decrease due to scattering from the sidewalls of the feature, while the angular width of the IEAD must decrease to minimize this scattering. The higher voltages required to achieve these outcomes translate to powers that are difficult to sustain on a continuous wave (CW) basis. Pulsing enables IEADs to extend to high energy with narrow angular spread and lower average power. Although HAR etching is primarily limited by the ion energy reaching the etch front, neutral fluxes must penetrate deep into the feature to passivate surfaces while low energy etch products must diffuse out of the feature, both processes of which have conductance limits. Using pulsed biases with low duty cycle (DC is the fraction of the period for which power is on) results in a portion of the pulsed period having low (or no) etching. During this time, neutral fluxes from the plasma can penetrate deep into or etch products leave the feature.[3,16]

Many dielectric etch applications use multifrequency biases with high frequency (HF) intended to control the magnitude of fluxes (neutral and ion) onto the wafer and the low frequency (LF) intended to control the IEAD onto the wafer.[17] In these systems, the IEAD also depends on the magnitude of the HF voltage and on the DC bias of the high frequency portion of the circuit due to HF contribution to the oscillation of the plasma potential. A system having more control over the IEAD is an inductively coupled plasma (ICP) with a VLF capacitive bias on the substrate. For an ICP having minimal capacitive coupling, there is little oscillation of the plasma potential from the ICP source, and the sheath characteristics over the wafer are dominated by the VLF bias. With a constant ICP source and sufficiently low bias frequency to reduce electron heating, the magnitude of fluxes onto the substrate would be constant.

Managing the IEAD onto the wafer during the pulse period consists of contributions from the bias-on portion of the period and the bias-off portion of the period. Consider an ideal case having a constant ICP source and a VLF pulsed bias. The pulsed bias has a bias-on period with constant voltage amplitude and a bias-off period where the RF voltage is zero. In principle, the IEADs should be distinct during the bias-on and bias-off periods. However, the charging and discharging of the blocking capacitor that produces the DC bias on the substrate, V_{DC}, interferes with the independence of the bias-on and bias-off periods. The persistence (or lack of persistence) of V_{DC} is an opportunity to customize the format of the IEAD onto the wafer during the entire pulsed period.

In this paper, we discuss results from a computational investigation of IEADs onto wafers produced in an ICP sustained in an $Ar/Cl_2/O_2$ mixture having a pulsed VLF bias of 250 kHz. These are conditions typically used for HAR etching of DTI structures. The goal is to investigate the consequences of pulsing parameters including pulse repetition frequency (PRF), duty cycle (DC), blocking capacitance, and focus ring electrical properties on IEADs onto the wafer during the bias-on and bias-off portions of the pulsed period. In particular, we discuss the time dependence of V_{DC} that in large part determines ion energies onto the wafer during the bias-off period. During the bias-on portion of the pulsed period, the magnitude of V_{DC} will increase (become more negative) due to the imbalance in current collected by the powered and grounded terminals of the circuit that charges the blocking capacitor (capacitance C_B). V_{DC} dissipates during the bias-off period in the absence of the applied RF voltage. At this time, it is only V_{DC} that maintains the sheath above the wafer. The charging and discharging of C_B that produces V_{DC} is ultimately a function of the effective RC (resistance • capacitance) time constant for the blocking capacitor, which, in turn, depends on the value of the blocking capacitor and impedance of the plasma and materials in contact with the substrate. The focus ring (FR) is a structure surrounding the substrate and wafer, which is intended to minimize edge exclusion by improving uniformity of the ion and radical fluxes across the wafer to the FR interface. The FR also represents an impedance between the substrate and plasma and so can provide an additional avenue for current flowing to the blocking capacitor, both during the bias-on and bias-off periods.

The model used in this investigation and the reactor conditions are described in Sec. II. Plasma properties for the base case are discussed in Sec. III. Consequences of varying pulsing parameters on V_{DC} and IEDs to the wafer are discussed in Sec. IV. The consequences of pulsing on angular tilt of the IED are discussed in Sec. V. Concluding remarks are in Sec. VI.

II. DESCRIPTION OF THE PLASMA REACTOR MODEL

The Hybrid Plasma Equipment Model (HPEM) was used to simulate the plasma dynamics in this work and is described in detail in Refs. 18 and 19. A brief summary is given here. The HPEM is a two-dimensional hydrodynamics model that utilizes modules that address different physical phenomena while iteratively transferring physical quantities to other modules. The primary modules used in this work are the Electromagnetics Module (EMM), Fluid Kinetics-Poisson Module (FKPM), Electron Energy Transport Module (EETM), and Plasma Chemistry Monte Carlo Module (PCMCM).

Electromagnetic fields produced by RF current passing through the antennas are calculated in the EMM using a frequency domain solution. The power deposition produced by the electromagnetic fields is transferred to the FKPM for use in solving the electron energy equation; and the electric and magnetic fields are transferred to the EETM and PCMCM.

Continuity, momentum, and energy equations for individual species are integrated in the FKPM, producing time-resolved neutral and charged particle densities, fluxes, and temperatures. Charged particle densities are obtained from their corresponding continuity equations solved concurrently with Poisson's equation to produce electrostatic potentials. The bulk electron flux is obtained from a Scharfetter–Gummel drift-diffusion model. Solving the stationary Boltzmann's equation using a two-term spherical harmonic solution for electron energy distributions (EEDs) then produces transport and rate coefficients for bulk electrons.

The electromagnetic fields from the EMM and the electrostatic fields from the FKPM are then transferred to the EETM, which uses Monte Carlo methods to calculate EEDs for sheath accelerated electrons produced by secondary emission from surfaces due to ion bombardment. From these EEDs, electron impact rate and transport coefficients are produced for the FKPM.

The PCMCM receives source functions for ions from the FKPM, electromagnetic fields from the EMM, and electrostatic fields from the FKPM. Using Monte Carlo methods, the PCMCM tracks pseudoparticle ion trajectories from the site of ion formation until the ion strikes a surface. Ion energy and angular distributions are then produced from the statistics of the ion striking surfaces.

The cylindrically symmetric ICP reactor used in this investigation is shown in Fig. 1. The reactor is powered by a flat four-turn antenna above a 1.5 cm thick dielectric alumina window with a gas injection shower head as a part of the window. A 300 mm diameter wafer (dielectric constant $\epsilon/\epsilon_0 = 12.5$, conductivity $0.01\ \mathrm{S\,cm^{-1}}$) was placed on top of the lower metal electrode, which was surrounded by and flush with an alumina focus ring of 3.75 cm width having a relative permittivity of $\epsilon/\epsilon_0 = 9.85$ and a conductivity of $10^{-6}\ \mathrm{S\,cm^{-1}}$. Gas was pumped out through an annular port surrounding the focus ring with 5.1 cm width, providing an internal diameter of the chamber of 47.6 cm. The chamber walls were grounded metal. The secondary electron emission coefficient due to ion impact for the wafer, dielectrics, and metals in contact with the plasma was 0.15, 0.10, and 0.02.

A feedstock gas of $Ar/Cl_2/O_2 = 90/9/1$ was supplied at 300 SCCM through the showerhead at the top of the reactor. The pressure was held constant at 15 mTorr at the entrance to the pump. The Ar/Cl_2 and Ar/O_2 portions of the reaction mechanism are the same as discussed in Refs. 20 and 21. Reactions between Cl_2 and O_2 feedstock gases are as described in Ref. 22.

RF power was supplied to the bias electrode through a blocking capacitor, C_B. For the system to reach a pulse-periodic steady

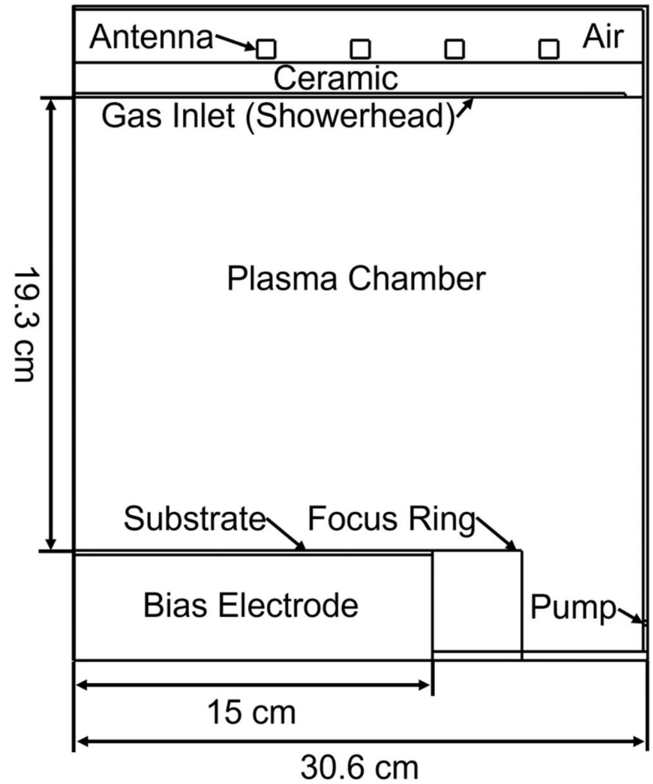

FIG. 1. Schematic of the ICP reactor. The biased substrate is connected to the RF power supply through a blocking capacitor.

state, V_{DC} must also reach a pulse-periodic steady state across bias pulse periods. V_{DC} may oscillate during a VLF period if the RC time constant for charging and discharging C_B is commensurate with the RF period.[23] The rate of charging and discharging of C_B is dependent on this RC time constant while the quasi-steady state value of V_{DC} with CW excitation is independent of the capacitance. Charging (and discharging) of C_B is due to the difference in currents collected by the powered electrode and current to ground. These currents (displacement and conduction) are computed at the surfaces of the metals on the powered and grounded sides of the circuit.[24–27]

The IEADs and IEDs discussed here are averages of the total ion flux (all ion species) onto the wafer during the bias-on and bias-off periods. Electric fields are recorded as a function of position and phase in the FKPM over the last pulse period. Those fields and source functions are used to launch and track the trajectories of the pseudoparticles in the PCMCM that strike the wafer, which are then recorded to produce the IEAD. In this implementation of the HPEM, the only role of the PCMCM is to compute the IEADs onto surfaces using test particles. The resulting IEADs do not feedback to other portions of the model and, in particular, do not feedback to the solution of Poisson's equation for the electrical potential.

The basic structure of the HPEM is to iterate through different physics models exchanging information between the modules with a period of τ_E which is typically 0.1–1 μs. When operating with a VLF bias, the RF period, τ_{RF}, may exceed τ_E, which then violates the hierarchy for data exchange between modules. To address these conditions, a low frequency pulsing option was developed that enables separately recording of electric fields during the pulse-on and pulse-off portions of the pulse period, which may extend over several τ_E exchange periods.

One of the goals of two-frequency capacitively coupled plasmas and ICPs with a capacitive substrate bias is to have separate control over ion fluxes and IEADs. This independent control can be challenging when bias powers are large compared to source powers or when bias power is held constant as opposed to bias voltage.[28] When holding bias power constant and changing source power, ion current varies, which then requires a change in bias voltage. Even with holding bias-voltage constant, changing source power varies plasma density, which then modulates sheath thickness, an important parameter in determining the IEAD. In order to minimize these effects and isolate the consequences of the pulse-power format, we have held both source power and bias voltage constant.

III. PLASMA PROPERTIES

Operating conditions for the base case are a gas mixture of $Ar/Cl_2/O_2 = 90/9/1$ at 15 mTorr with a flow rate of 300 SCCM, a constant ICP power of 500 W at 10 MHz, and a 250 kHz bias on the substrate having a constant 1 kV voltage amplitude when the bias power is on. C_B has a value of 100 nF. The electron density and electric potential are shown in Fig. 2. The formation of V_{DC} is shown after turning on the LF bias. The maximum electron density is 6.9×10^{10} cm^{-3}, with the ratio of ion densities at the site of the maximum density being $Ar^+/O_2^+/Cl^+/Cl_2^+ = 13/1/6/80$. In addition to the mole fractions of the feedstock gases, which favor ionization of Ar and Cl_2, charge exchange reactions (ionization potentials in ascending order are Cl_2^+, O_2^+, Cl^+, O^+, and Ar^+) favor the formation of Cl_2^+. The electric potential is uniform across the majority of the wafer, with curvature over the wafer to dielectric focus ring boundary due to charging of the FR that thins the sheath above the FR. Since the RC time constant for charging the FR of $\approx$2.5 μs is less than the 4 μs RF period at 250 kHz, the capacitance of the FR fully charges during the RF bias period. V_{DC} reaches a cycle average steady state of −620 V, while there is an oscillation of ±40 V during the RF cycle. This oscillation is due to the RC time constant for charging C_B being less than but still a significant fraction of the RF period. The IEAD averaged over the wafer is shown in Fig. 2(d). The steady state V_{DC} of −620 V contributes to the maximum energy of the IEAD being close to 1600 eV. The angular width of the IEAD is largest at the highest energy due to the sheath being at its maximum extent with the largest sheath voltage. Ions transporting from the maximum in the plasma density [Fig. 2(a)] then enter the extended sheath with a diverging velocity. This effect is a consequence of this particular geometry and is not a general trend.

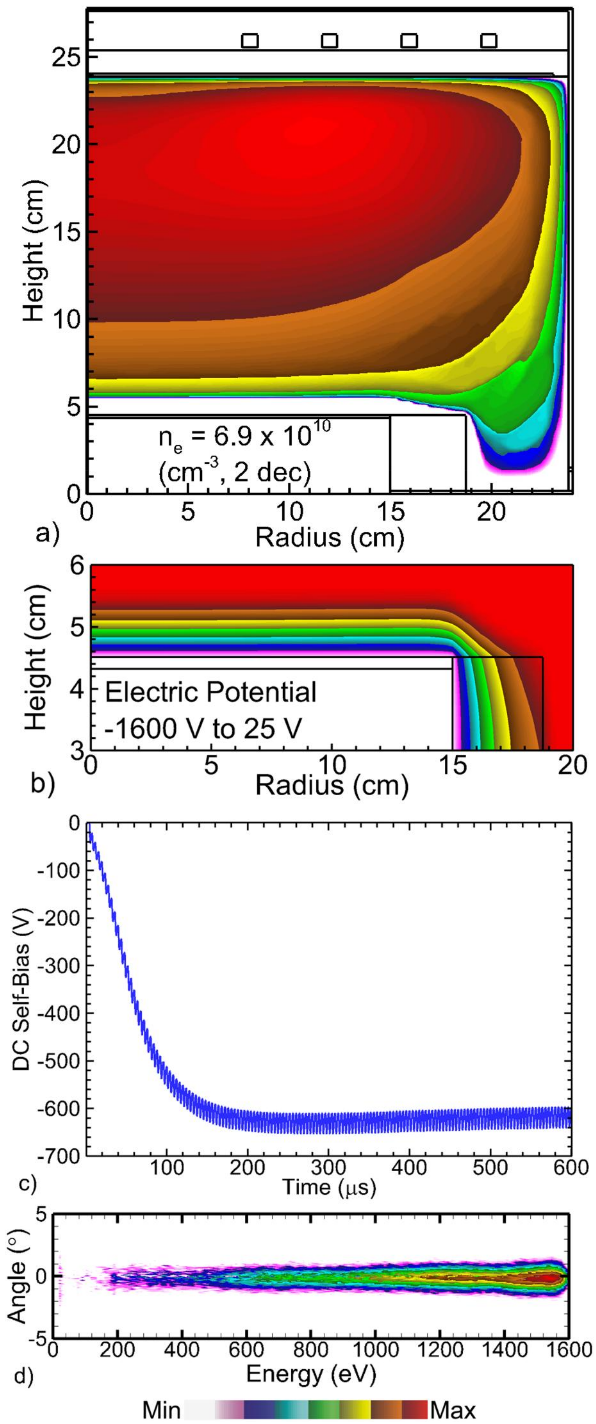

FIG. 2. Plasma properties for the base case with a CW 250 kHz bias. (a) Electron density (two-decade log scale), (b) electric potential at the maximum negative bias, (c) time evolution to the steady state of V_{DC} after turning on the bias, and (d) IEAD incident onto the wafer plotted over two decades. The maximum value is noted in each image with the range of decades for log plots.

IV. IMPACT OF VLF BIAS PULSING ON V_{DC} AND ION DISTRIBUTIONS TO THE WAFER

In this section, the impact of VLF bias pulsing on V_{DC} and ion distributions to the wafer will be discussed as a function of pulse repetition frequency, duty cycle, blocking capacitance, and focus ring properties. These trends are collated and discussed in Sec. IV E.

A. Pulse repetition frequency

The formation and dissipation of V_{DC} during the RF period for different PRFs for a DC of 50% are shown in Fig. 3. The RF bias frequency is 250 kHz. The RC time constant for charging and discharging C_B when changing PRF is approximately the same, 2.5 μs. With the capacitance being held constant and the plasma conductivity being determined dominantly by the ICP power, the RC time constant remains nearly the same. Over this range of PRFs, we see two extremes. For PRFs less than ≈8.5 kHz (period >120 μs), V_{DC} is both fully formed during the bias-on portion of the pulse and fully dissipated by the end of the bias-off period. The start of each pulse begins generating V_{DC} anew during the longer pulse period. The end result is a broad range of V_{DC} values over the pulse period for a given PRF. For PRFs greater than ≈8.5 kHz (period <120 μs), V_{DC} does not fully develop and does not fully dissipate during the pulse period. These conditions result in the range of V_{DC} being narrower over the shorter periods.

The RF period is long enough that the thin sheath limit applies, which, in turn, produces a wide range of ion energies independent of the PRF for pulsing. IEADs incident onto the wafer averaged over the bias-on and the bias-off portions of the pulse for a selection of PRFs (2 to 50 kHz) are shown in Fig. 4 for the conditions corresponding to Fig. 3 (RF 250 kHz and duty cycle 50%). The IEDs (averaged over angle) incident onto the wafer averaged over the bias-on and bias-off periods for several more PRFs are shown in Fig. 5. The mean and peak-maximum ion energies incident onto the wafer are shown in Fig. 3(c). *Peak-maximum* energy refers to the energy at which the IEAD has its maximum value, which may not be the maximum energy of ions incident onto the wafer. The peak-maximum energy is the most likely energy incident onto the wafer.

With the sheath being in the thin-sheath limit, the IEADs (IEDs) are bimodal—ions cross the sheath in a time that is short compared to the RF period. In the absence of collisions, ions strike the wafer with an energy nearly equal to the sheath potential when they enter the sheath. During the bias-on period, the high energy peak represents the maximum sheath potential ($V_{RF} - V_{DC}$) occurring during the cathodic portion of the RF cycle. The low energy peak during the anodic portion of the cycle represents the magnitude of the plasma potential produced by the ICP power deposition. The IEAD (and IED) during the bias-off period is determined dominantly by the time variation in V_{DC}. If V_{DC} does not fully discharge during the bias-off period, the range of ion energies will be bounded by the minimum and maximum values of V_{DC}. If V_{DC} is fully discharged during the bias-off period, the IEAD (and IED) will have a low energy peak that again reflects the plasma potential produced by the ICP power.

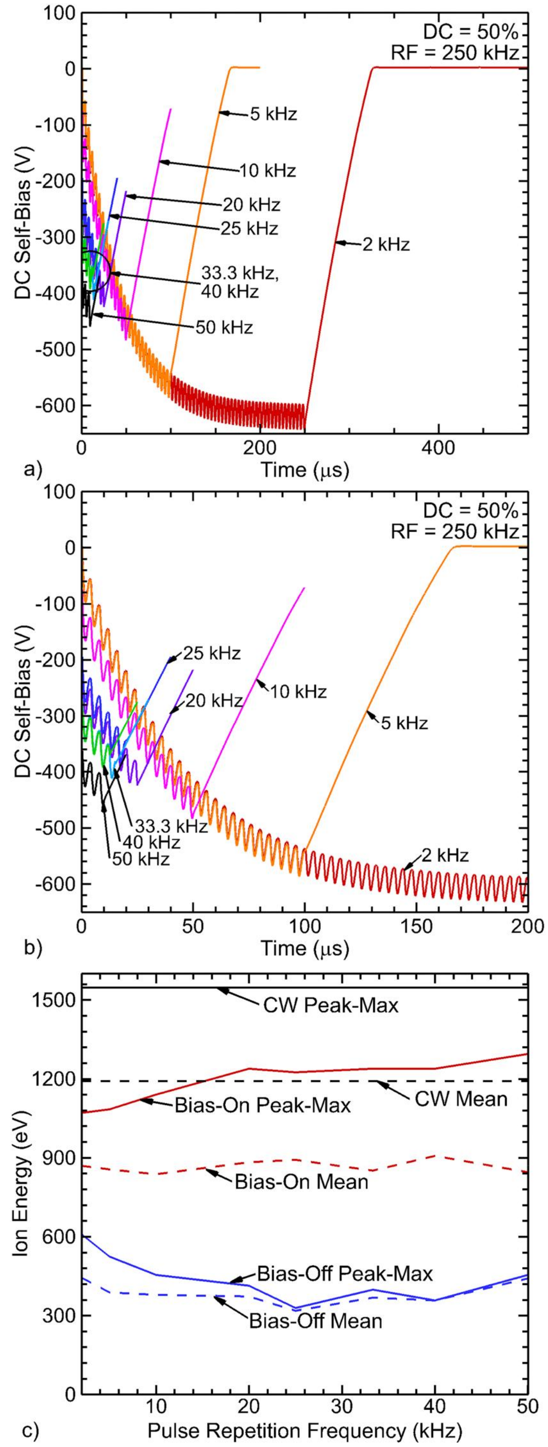

FIG. 3. Bias properties as a function of PRF for a 50% duty cycle with a 250 kHz RF bias. (a) V_{DC} during a full pulse period and (b) V_{DC} at early times during the pulse period. (c) Mean and peak-maximum ion energies onto the wafer during the bias-on and bias-off periods.

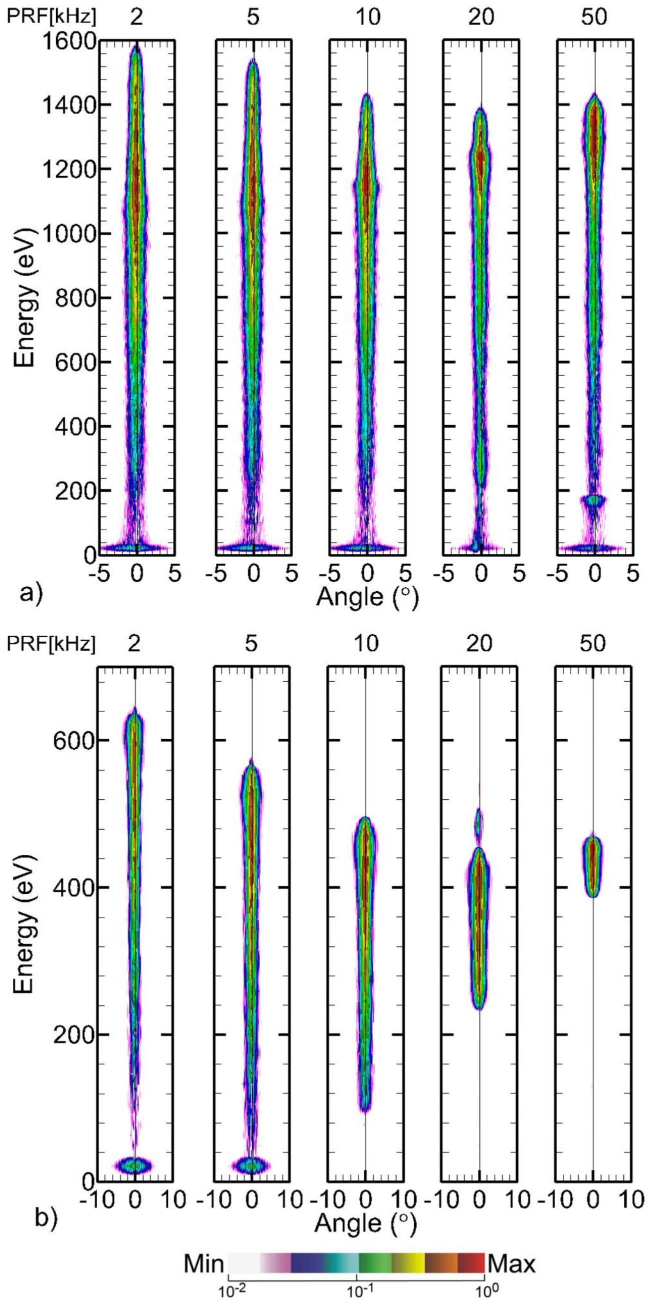

FIG. 4. Ion energy and angular distributions onto the wafer for pulse repetition frequencies of 2–50 kHz for a 50% duty cycle and a bias frequency of 250 kHz averaged over (a) bias-on and (b) bias-off periods. Images are plotted on a two-decade log scale.

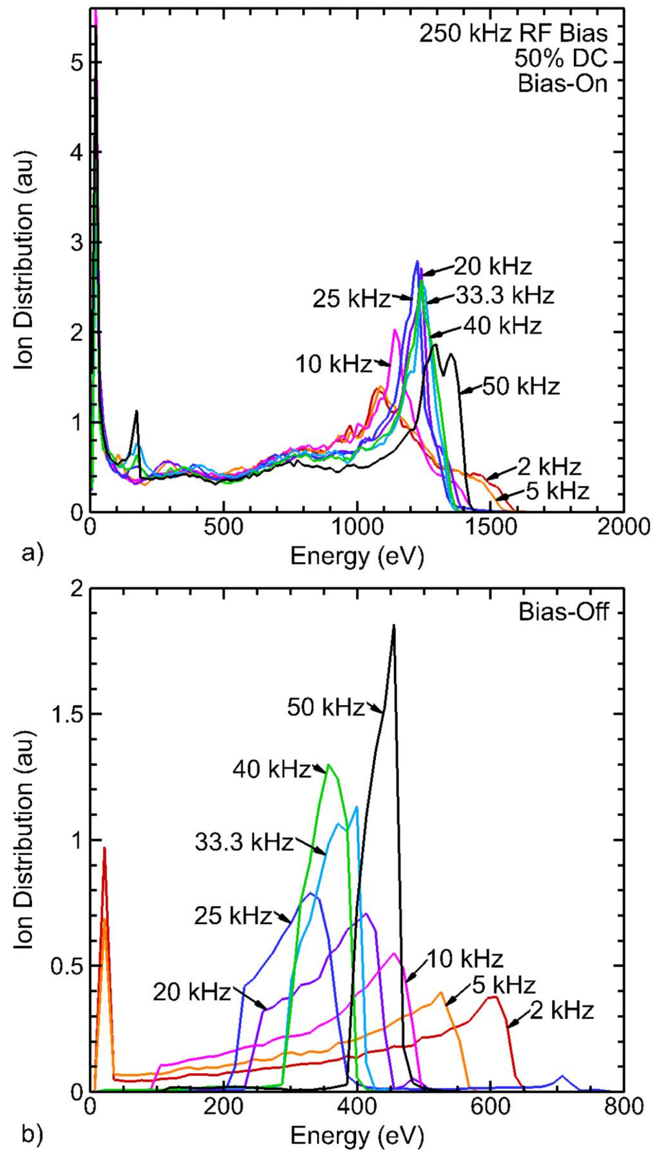

FIG. 5. Ion energy distributions onto the wafer for pulse repetition frequencies of 2–50 kHz for a 50% duty cycle and a bias frequency of 250 kHz averaged over (a) bias-on and (b) bias-off portions of the pulsed period.

The IEAD (and IED) averaged over the pulse period for 2 kHz has the maximum energy, 1600 eV, due to V_{DC} reaching a quasi-steady state during the longer period. However, since the V_{DC} is fully discharged by the end of the bias-off phase, charging of V_{DC} during the following pulse begins from essentially zero voltage. As V_{DC} charges up during the pulse period, ions striking the wafer have progressively higher energies. When averaged over the bias-on portion of the pulse, the energy at which the IEAD (and IED) is maximum is shifted to lower energy. At high PRF, the dynamic range of V_{DC} during the pulse period is less than 100 V with a mean of about −400 V, resulting in a narrower high energy peak to the IEDs. At low PRF, V_{DC} varies from essentially 0 to −640 V, which then enables the IED to extend to higher energies but with lower fluxes.

The angular spread of the IEAD at 50 kHz has a full width at half maximum of 0.77°, narrower than the angular spread at 2 kHz of 0.92°. This narrowing of the angular distribution, though small, results from V_{DC} maintaining a large negative value (−400 V) for the entire pulse period at 50 kHz. At 2 kHz, the full discharge of V_{DC} results in the bias-on portion of the pulse beginning without a DC bias and so with a smaller sheath potential. Larger sheath potentials generally produce more narrow angular distributions.

The dynamics of V_{DC} do have an impact on the energy and angular distributions onto the wafer and the average of ion energies onto the wafer during the bias-on portion of the pulse. That said, there are no significant differences in IEADs (and IEDs) as a function of PRF during the bias-on portion of the pulse in the thin-sheath limit.

The IEADs (and IEDs) during the bias-off period have a more sensitive dependence on PRF. At high PRF (short period), there is not sufficient time for V_{DC} to dissipate during the shorter bias-off period, and so there is a significant sheath potential during the bias-off phase. This nearly constant sheath potential produces an IEAD (and IED) during the bias-off period having a narrow energy spread centered on the persistent value of V_{DC}. With decreasing PRF (both longer bias-on and bias-off), V_{DC} both charges to a higher value and discharges to a lower value. The result is that the IEAD (and IED) during the bias-off period broadens in energy. For PRFs of 5 kHz and smaller, V_{DC} reaches a more negative value during the bias-on period producing higher energy ions, but V_{DC} also fully discharges during the bias-off period. Fully discharging V_{DC} results in the plasma potential being due to the inductive power, producing a low energy peak to the IED of 21 eV. As the PRF increases, maximum and mean energies of ions striking the wafer converge during the bias-off period, as shown in Fig. 3(c), in alignment with the narrowing in energy of the IED shown in Figs. 4 and 5.

The IEDs discussed here are averages over the bias-on and bias-off portions of the pulsed period. An example of the dynamics of the IEDs during the bias-off period is in Fig. 6 for the 10 kHz case in Fig. 5. With the RF bias-off and the substrate potential due only to the DC bias, the IED at any instant during the bias-off period is narrow in energy. The energy width of the IED is determined by the ICP sustained plasma potential at the location in the reactor from which the ions originate. We acknowledge that the outcome of the etch process resulting from the broad average IED may differ from that resulting from the sequence of narrow IEDs during the bias-off period. We also expect that these differences will be highly case specific.

B. Duty cycle

Similar to the length of the pulse period determined by PRF, the degree of charging and discharging of the blocking capacitor, and value of V_{DC}, can be controlled by varying the DC of the pulse. V_{DC} as a function of time is shown in Fig. 7(a) for an RF bias at 250 kHz and a PRF of 10 kHz for DCs of 10%–90%. The corresponding peak-maximum and mean ion energies to the wafer are in Fig. 7(b). The IEDs onto the wafer during the bias-on and bias-off period are in Fig. 8. V_{DC} fully dissipates during the bias-off period for DCs below 50%, leaving the sheath potential at about 20–25 V for an increasing larger fraction of the pulse as the DC decreases. At higher DC, there is a nonzero but varying value of V_{DC} throughout the entire pulse period. A DC of >80% is required to fully charge the blocking capacitor to its steady state value. Both mean and maximum ion energies onto the wafer scale nearly linearly with increasing DC as shown in Fig. 7(b).

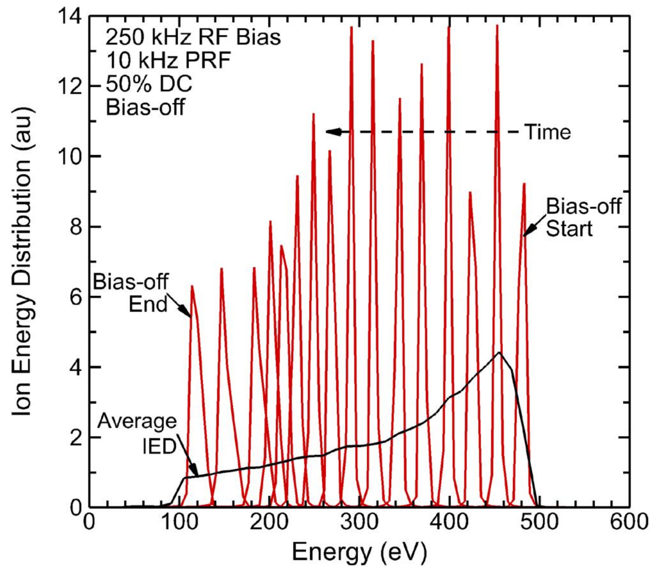

FIG. 6. IEDs during the bias-off period for a PRF of 10 kHz, 250 kHz RF bias and 50% DC. IEDs are shown from the start of the bias-off period to the end of the bias-off period. The IED averaged over the bias-off period is shown for comparison.

The IEDs reflect the dynamic range in V_{DC} resulting from varying DC. For large DC, the longer charging time for V_{DC} extends the bias-on IED to energies exceeding 1600 eV while reducing the low-energy peak. Also at large DC, the persistence of and lack of discharging of V_{DC} produces a narrow IED during the bias-off period, albeit for a short period of time. With a smaller DC, the maximum magnitude of V_{DC} is smaller (shorter charging time) and the discharging of V_{DC} is more complete. The end result is a decrease in the maximum energy and broadening of the IED during the bias-off period. With full discharging of V_{DC} for DCs less than 40%, the low energy peak of the IED (corresponding to the ICP produced plasma potential) increases in magnitude.

C. Blocking capacitance

With CW excitation, the RF cycle average value of V_{DC} is independent of the capacitance of the blocking capacitor. When pulsing, the charging and dissipation of V_{DC} depend on the effective RC time constant, a function of both the blocking capacitance and the conductivity of the bulk plasma through which V_{DC} discharges. By varying the capacitance of the blocking capacitor, one controls the rates of charging and discharging of V_{DC}. With the amplitude of the RF voltage remaining constant, pulsing the capacitance C_B then provides an adjustable offset to the IEDs.

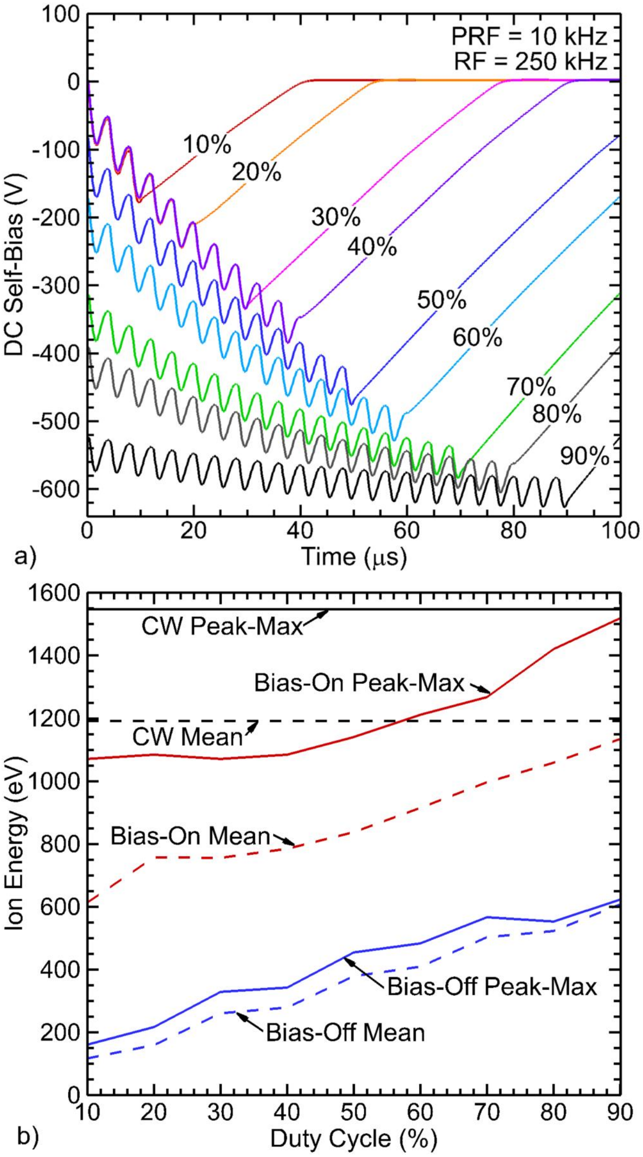

FIG. 7. Bias properties as a function of duty cycle for a PRF of 10 kHz and a 250 kHz RF bias. (a) V_{DC} during a full pulse period. (b) Mean and peak-maximum ion energies onto the wafer during the bias-on and bias-off periods, compared to the CW average value.

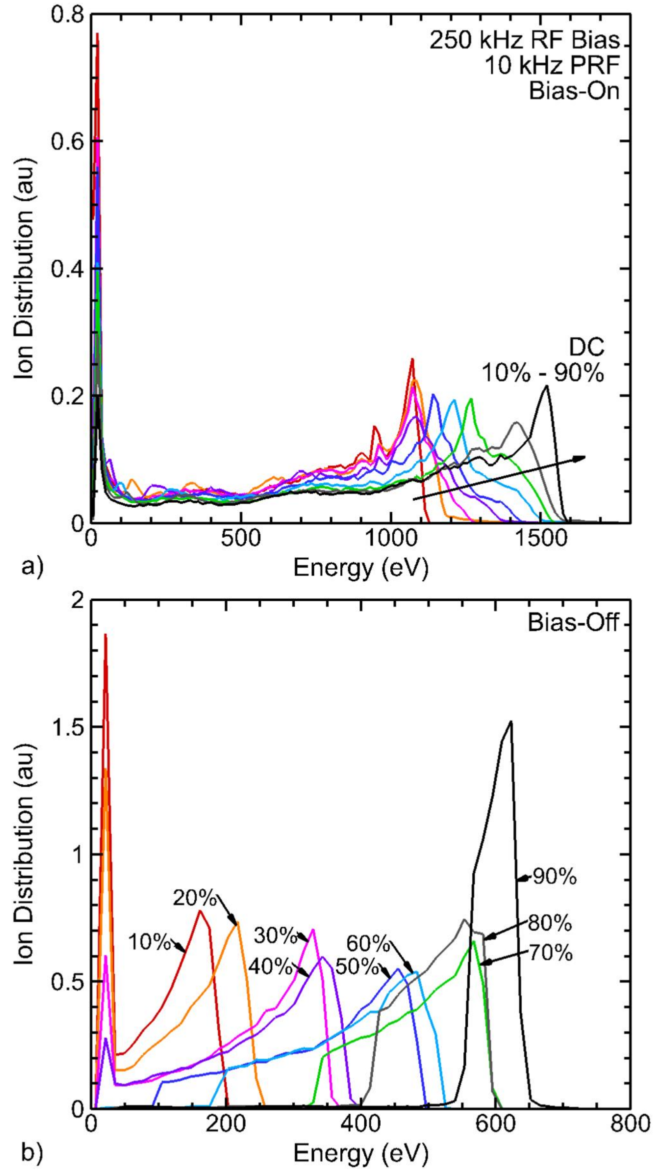

FIG. 8. Ion energy distributions onto the wafer for duty cycles of 10%–90% for a PRF of 10 kHz and a RF bias frequency of 250 kHz averaged over (a) bias-on and (b) bias-off portions of the pulsed period.

For example, V_{DC} and ion energies are shown in Fig. 9 for a PRF of 10 kHz and a duty cycle of 50% while varying the blocking capacitance, C_B, from 100 to 1000 nF. With $C_B = 100$ nF, the oscillation of V_{DC} during the RF cycle is tens of volts. The maximum value of V_{DC} reaches −490 V while discharging to −75 V during the bias-off phase. With $C_B = 1000$ nF, the oscillation of V_{DC} during the RF cycle is only a few volts, while the maximum V_{DC} reaches only −150 V, discharging to only −130 V during the bias-off phase.

IEDs averaged over the bias-on and bias-off periods as a function of C_B are shown in Fig. 10. Their maximum and mean energies as a function of C_B are shown in Fig. 9(b). With the largest excursion of V_{DC} being with the smallest value of C_B, the IED during pulse-on extends to the highest energy with $C_B = 100$ nF. The low energy portion of the IEAD that is collected during the anodic portion of the RF period is essentially independent of C_B. With ion acceleration operating in the thin-sheath limit, ions carry little memory of the sheath properties during the

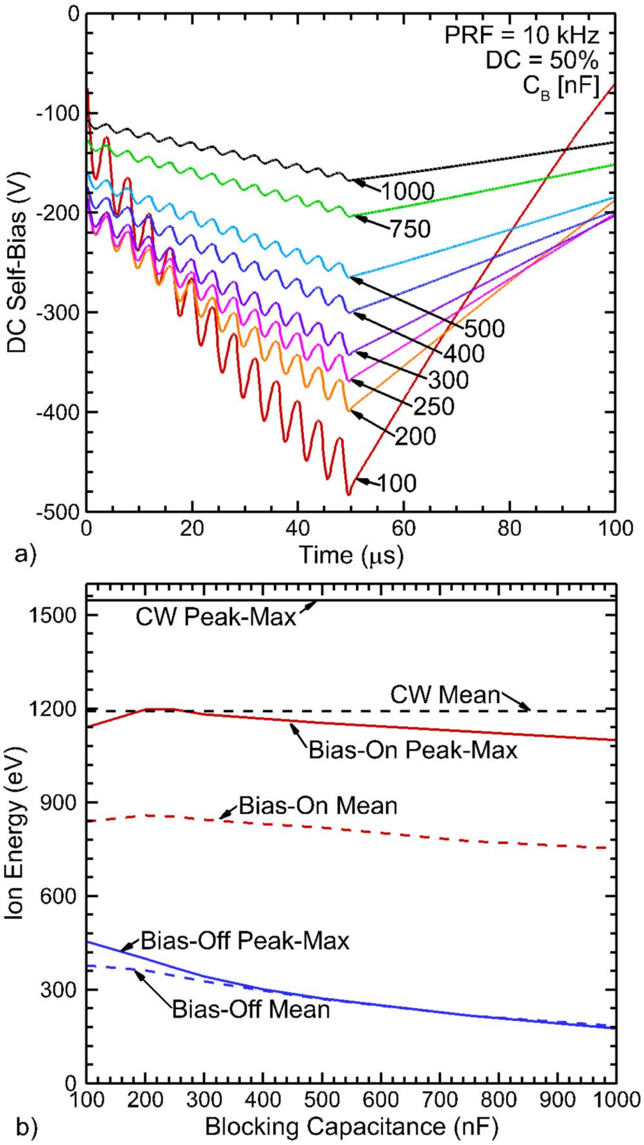

FIG. 9. Bias properties as a function of blocking capacitance for a duty cycle of 50%, PRF of 10 kHz, and a 250 kHz RF bias. (a) V_{DC} during a full pulse period. (b) Mean and peak-maximum ion energies onto the wafer during the bias-on and bias-off periods, compared to the CW average value.

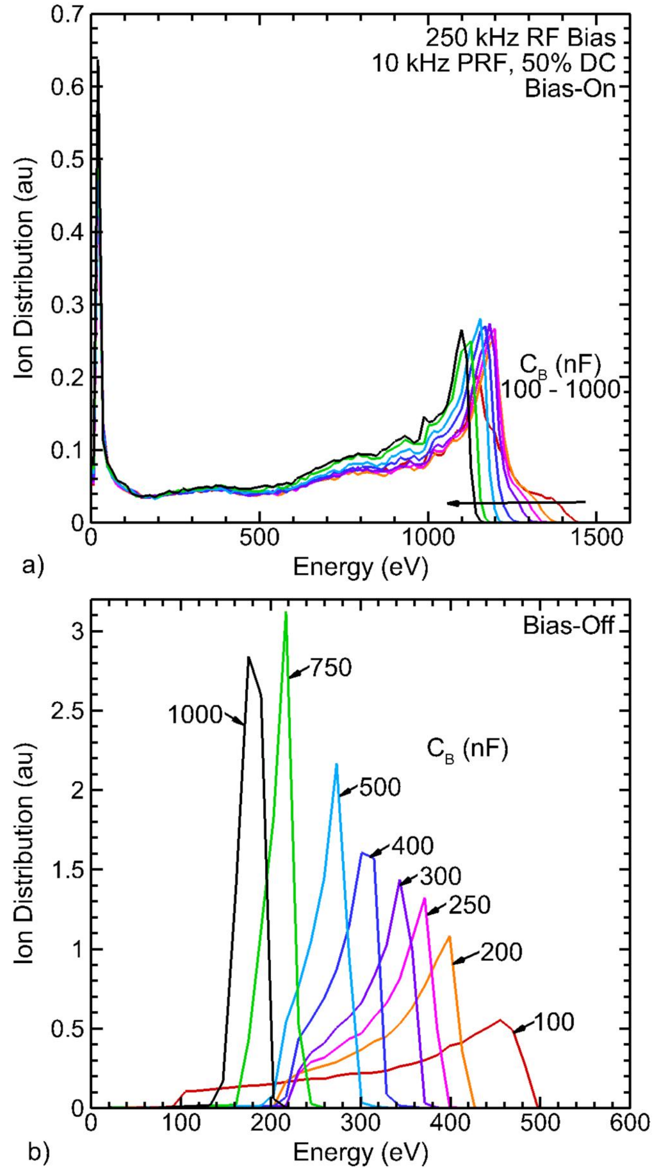

FIG. 10. Ion energy distributions onto the wafer for blocking capacitances of 100–1000 nF for a 50% duty cycle, a PRF of 10 kHz, and a RF bias frequency of 250 kHz. IEDs are shown averaged over (a) bias-on and (b) bias-off portions of the pulsed period.

cathodic phase when the magnitude of V_{DC} adds to the sheath potential. With the electron temperature and density also being nearly independent of C_B, the anode sheath, which is largely a function of the electron thermal flux into the sheath, is also nearly independent of C_B.

The IEDs averaged over the bias-off periods are strongly modulated by the value of C_B. Large values of C_B produce a small magnitude of V_{DC} while also having a small variation during the RF cycle. These conditions produce an IED during the bias-off phase that is low energy and narrow in width. Small values of C_B for which the magnitude of V_{DC} is large while also having a large variation during the RF cycle produce an IED during the bias-off that is broad in energy, extending to high energy.

Pulsing the bias typically has the goal of delivering IEADs with high energy during the bias-on period and low energy during the pulse-off period. The dependence of V_{DC} on C_B suggests that these goals are met by choosing either very large or very small values of C_B. Large values of C_B may not deliver the highest ion energy during the bias-on but does deliver the lowest average ion energy during the bias-off period. Small values of C_B will deliver the highest ion energies during the power-on. However, to minimize the ion energies delivered during the bias-off period, the length of the bias-off period must significantly exceed the RC time constant for discharging C_B.

D. Focus ring properties

The current flowing to the blocking capacitor has two components—current flowing through the wafer and current flowing through the focus ring. The conduction current flowing through the wafer to the electrode is limited by the series resistance of the wafer and sheath, whereas the displacement current flowing through the wafer is limited by the series reactance of the wafer and sheath. The current through the focus ring is similarly limited. However, with most focus rings being dielectric or materials with low conductivity (high resistivity), the current flowing through the focus ring is dominantly displacement current. The displacement current is, in turn, dependent on the permittivity of the focus ring.

V_{DC} and ion energies during the pulse period are shown in Fig. 11 for values of relative permittivity, ϵ_r, of the FR permittivity of 9.85–100. IEDs averaged over the bias-on and bias-off portions of the cycle are shown in Fig. 12. The blocking capacitance is 100 nF, PRF is 10 kHz, and duty cycle is 50%. Although ϵ_r of the FR can significantly affect the sheath structure at the wafer-FR boundary and so control the angular tilt of the IEAD at the edge of the wafer,[29,30] the permittivity of the FR has little effect on the dynamics of V_{DC}. Larger values of ϵ_r (larger capacitance of the FR) enable more displacement current to flow through the FR to the blocking capacitor prior to the capacitance of the FR fully charging. With more displacement current flowing to the blocking capacitance, the oscillation in V_{DC} is greater with larger values of ϵ_r, although this is not a big effect. From $\epsilon_r = 9.85$ to 100, the oscillation in V_{DC} changes by only a few tens of volts. The end result is that IEDs during both the bias-on and bias-off phases depend weakly on ϵ_r.

For the conditions of this investigation, charging and discharging of the blocking capacitance are dominated by current collected directly by the wafer, which has a lower impedance than that of the FR. The permittivity of the FR is then not particularly influential on the dynamics of V_{DC}. Another electrical property of the FR is conductivity, which would provide a conduction current path through the FR to C_B. V_{DC} during the pulsed period is shown in Fig. 13 for FR conductivities of 10^{-6}–10^{-3} S/cm. The general trend is that V_{DC} becomes less negative with increasing conductivity of the FR. With V_{DC} being negative, the effective current-collecting area of the substrate appears smaller than that on the grounded side of the circuit. [Recall that V_{DC} scales with the ratio of the effective current-collecting areas on the powered and grounded sides of the circuit—$(A_1/A_2)^n$.] With increasing conductivity of the FR, the surface area delivering conduction current to the blocking capacitors increases, which, in turn, decreases the magnitude of V_{DC}.

The decrease in the magnitude of V_{DC} (becoming less negative) with increasing conductivity of the FR reaches a lower limit

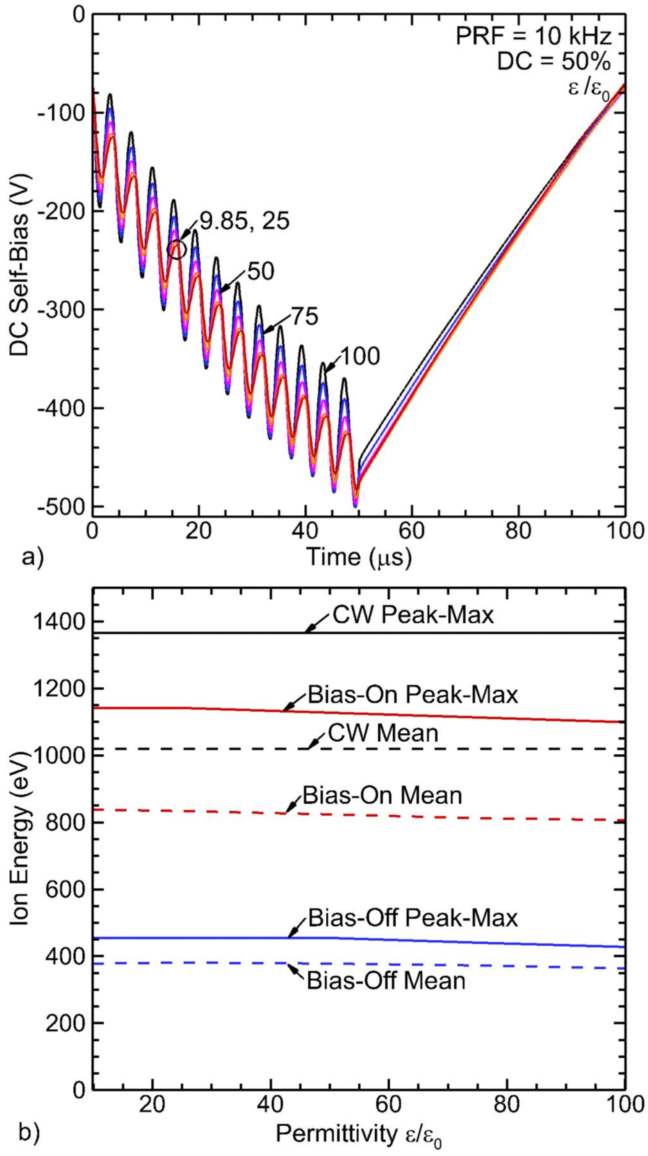

FIG. 11. Bias properties as a function of relative permittivity of the focus ring for a duty cycle of 50%, a PRF of 10 kHz, and a 250 kHz RF bias. (a) V_{DC} during a full pulse period. (b) Mean and peak-maximum ion energies onto the wafer during the bias-on and bias-off portions of the period, compared to the CW average value.

at a conductivity of 10^{-4} S/cm. For lower conductivities, delivery of current through the FR to the blocking capacitor is limited by the impedance of the FR. For conductivities of 10^{-4} S/cm and higher, the delivery of current through the FR to the blocking capacitor is limited by the current incident onto the surfaces of the FR. (That is, the impedance of the sheath bounding the FR is larger than that of the FR.) The rate of discharge from the smaller

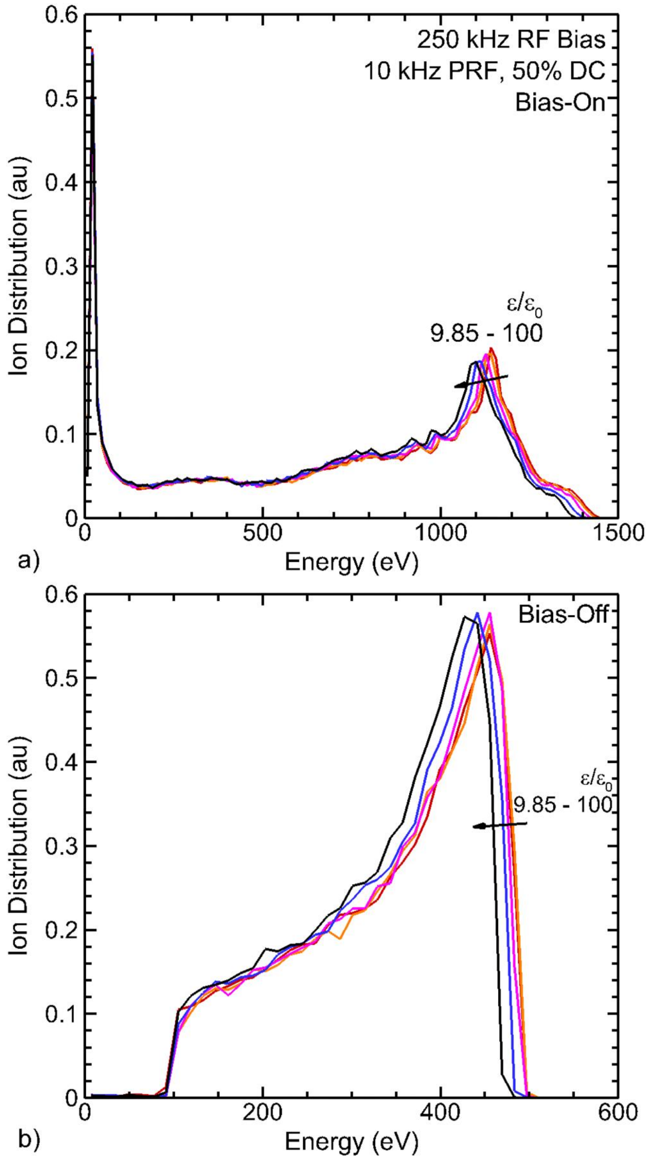

FIG. 12. Ion energy distributions onto the wafer for different relative permittivity of the focus ring for a 50% duty cycle, a PRF of 10 kHz, and a RF bias frequency of 250 kHz averaged over (a) bias-on and (b) bias-off portions of the pulsed period.

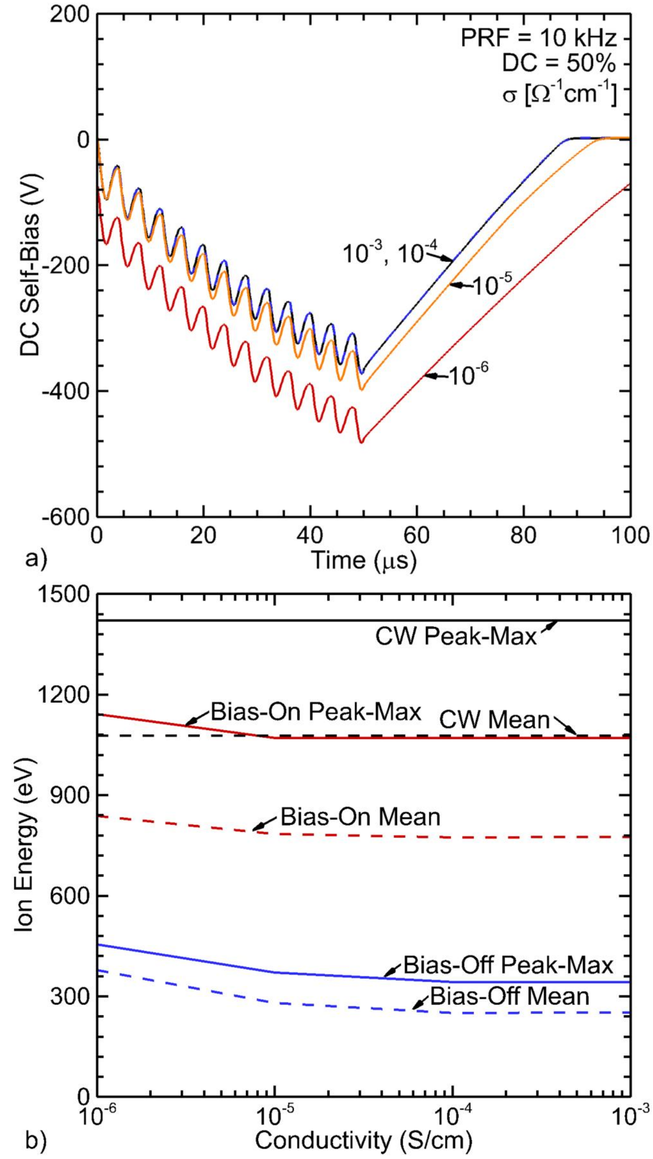

FIG. 13. Bias properties as a function of conductivity of the focus ring for a duty cycle of 50%, a PRF of 10 kHz, and a 250 kHz RF bias. (a) V_{DC} during a full pulse period. (b) Mean and peak-maximum ion energies onto the wafer during the bias-on and bias-off periods, compared to the CW average value.

magnitude of V_{DC} increases with increasing conductivity of the FR, enabling the blocking capacitor to fully discharge for the higher values of conductivity.

IEDs delivered to the wafer averaged over the bias-on and bias-off phases are shown in Fig. 14 for different values of FR conductivity. The IEDs averaged over the bias-on phase are weakly dependent on conductivity, with the exception of a progressive decrease in maximum energy with increasing conductivity. This decrease in maximum energy tracks the decrease in the magnitude of V_{DC}. With the full discharge of V_{DC} during the bias-off phase with higher conductivities, IEDs averaged over the bias-off phase have a dominant low energy component. It is only for the least conductive FR that V_{DC} does not fully discharge and whose IED is offset from 0 by about 100 eV.

The FR surrounding the powered electrode provides an additional parallel path for the current flow that can impact the

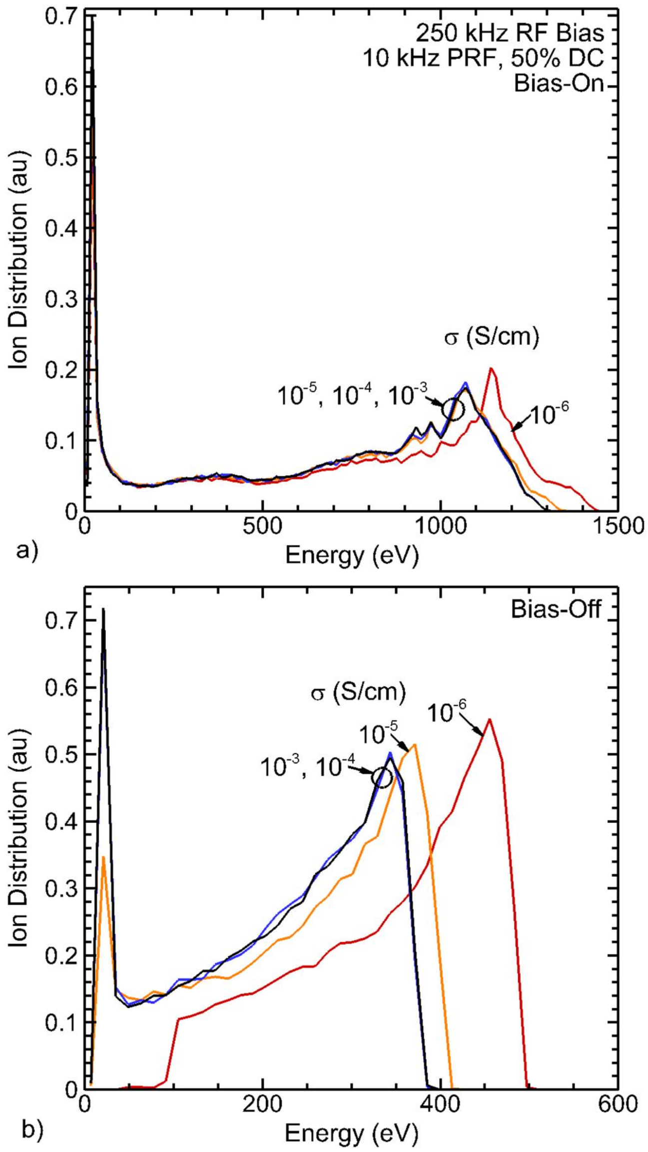

FIG. 14. Ion energy distributions onto the wafer for different conductivities of the focus ring for a 50% duty cycle, a PRF of 10 kHz, and a RF bias frequency of 250 kHz averaged over (a) bias-on and (b) bias-off portions of the pulsed period.

current contributions to the formation of V_{DC}. When the substrate is powered, current collected by the substrate through the wafer has both conduction and displacement current contributions. That collected through the focus ring is dominantly displacement current. During the bias-off phase, the current is dominated by conduction current through the wafer, as in the absence of RF oscillation, the displacement current through the FR is small. Since the total current collected by the substrate is dominated by that through the wafer, changing the permittivity of the FR does not significantly change the total current and so does not significantly change V_{DC}. However, when increasing the conductivity of the FR, a conduction current path through the FR is enabled, which is active during the bias-off period. This additional conduction current path is consequential on V_{DC}.

E. Scaling of peak-maximum energy

The parametric studies discussed above reflect the complexity faced in plasma equipment and process design. It is rare that a plasma property, such as IEAD onto the wafer, can be uniquely controlled with a single design parameter. To provide additional cohesion to the parametric results, the computed trends are collated in Fig. 15. The maximum energies of the IEAD during the bias-on period [Fig. 15(a)] and bias-off period [Fig. 15(b)] are plotted for varying (color coded) DC, pulse repetition rates (PRF), blocking capacitance C_B, focus ring conductivity (σ), and focus ring permittivity (ϵ/ϵ_0). The symbol is the average V_{DC} over the bias-on or bias-off period. The horizontal bars denote the range of V_{DC} during the bias-on or bias-off period.

During both the bias-on and bias-off periods, the maximum ion energy follows the magnitude of V_{DC} as expected, with the dynamic range of the ion energy being greatest with variation in DC, followed by PRF and blocking capacitance (C_B). These parameters are most closely related to the lengths of the bias-on and bias-off periods compared to the RC time constant for charging or discharging C_B. The dynamic range in ion energy depends less strongly on the FR properties, as these properties are less directly linked to the charging and discharging of C_B. With the ion energy being determined dominantly by the dynamics of V_{DC} during the bias-off period, there is a closer correlation between ion energies with V_{DC} than during the bias-on period when V_{DC} is augmenting the applied RF potential.

V. TILT OF THE IED AT THE WAFER EDGE

A previous study investigated the consequences of the FR electrical characteristics and their possible impact on sheath curvature at the interface of the wafer and FR.[10] An outcome of that investigation is that charging of the FR produces a thinner sheath above the FR compared to above the wafer. This disparity in sheath thickness across the transition between the wafer and FR produces curvature in the sheath. This curvature then produces a tilt away from the normal in the trajectories of ions incident onto the edge of the wafer. Minimizing the tilt in the ion trajectories at the edge of the wafer is important to reducing edge exclusion.

The impact of changes in FR electrical properties on the sheath curvature across the wafer-to-FR interface is shown in Fig. 16. The electric potential is shown during the bias-on period at the maximum of the cathodic potential and for the maximum V_{DC} during the bias-off period. For an FR with low conductivity, larger permittivity results in lower electric fields within the FR and more charge in its surface, both of which produce a thicker more extended sheath over the FR. The more extended sheath produces less sheath curvature at the edge of the wafer. Sheath curvature can be largely eliminated by having a sufficiently conductive FR that the FR supports little voltage drop.

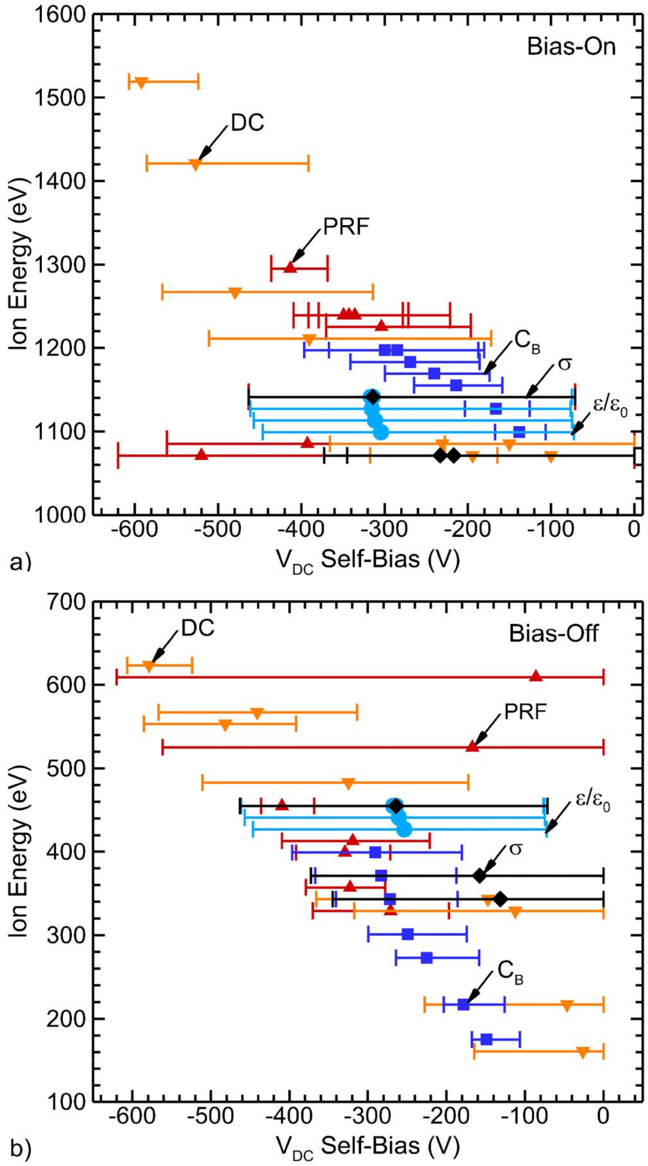

FIG. 15. Peak-maximum ion energy as a function of V_{DC} for all parametric conditions (parameters color-coded: DC = duty cycle, PRF = pulse repetition frequency, C_B = blocking capacitance, σ = focus ring conductivity, ϵ/ϵ_0 = focus ring permittivity). The average value of V_{DC} is noted by the symbol, and the range of V_{DC} is indicated by the far. (a) Bias-on and (b) bias-off.

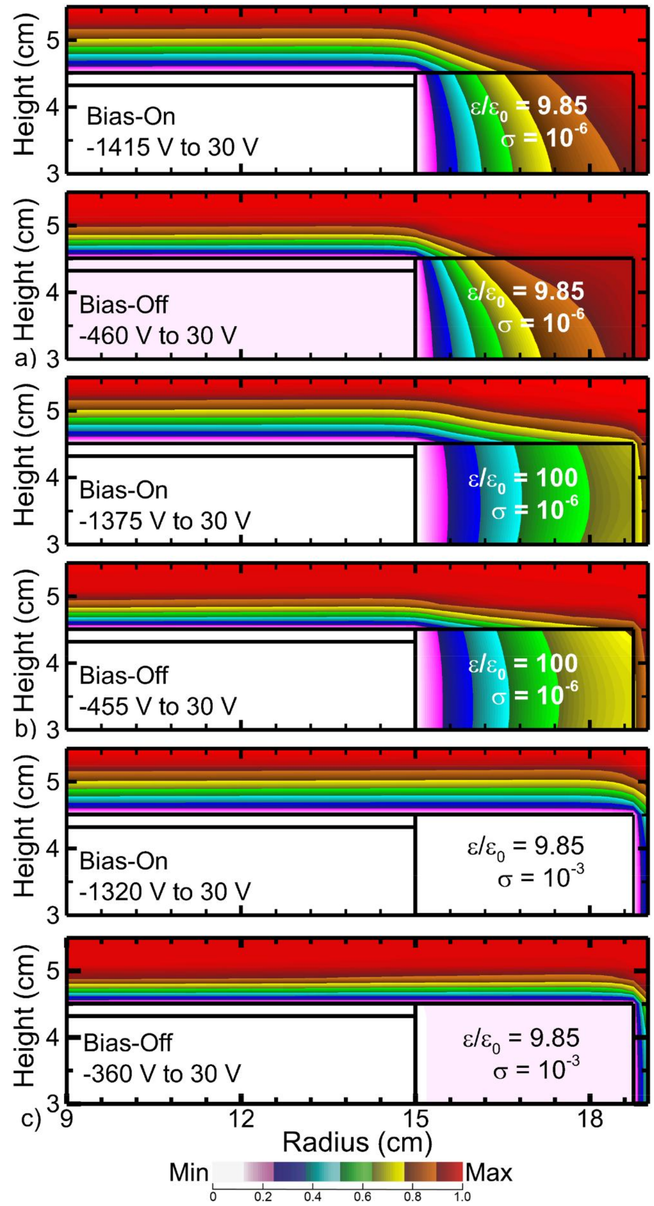

FIG. 16. Electric potential for bias-on at the peak cathodic (most negative) portion of the RF cycle and beginning of the bias-off period. Results are shown for focus ring permittivities and conductivities of (a) 9.85 and 10^{-6} S/cm, (b) 100 and 10^{-6} S/cm, and (c) 9.85 and 10^{-3} S/cm. Plasma conditions are 10 kHz PRF, 50% DC, and 250 kHz RF bias frequency.

Ion angular distributions (IADs) at the edge of the wafer for the bias-on and bias-off phases for different FR properties are shown in Fig. 17. For the base case ($\sigma = 10^{-6}$ S/cm, $\epsilon/\epsilon_0 = 9.85$), the mean angular skew during the bias-on portion of the cycle is 2° (full width-half maximum FWHM = 4°) pointing inward. When increasing permittivity to $\epsilon/\epsilon_0 = 100$, which produces less sheath curvature, the angular skew decreases to 1° (FWHM = 3°). With high conductivity (10^{-4} S/cm), the angular skew is 0.5° (FWHM = 1°) pointed outward. The high conductivity of the FR produces a slightly thicker sheath above the FR, which produces outward curvature.

With bias-off, the average angular skews are similar to the skews with bias-on. However, the FWHM of the IADs is larger.

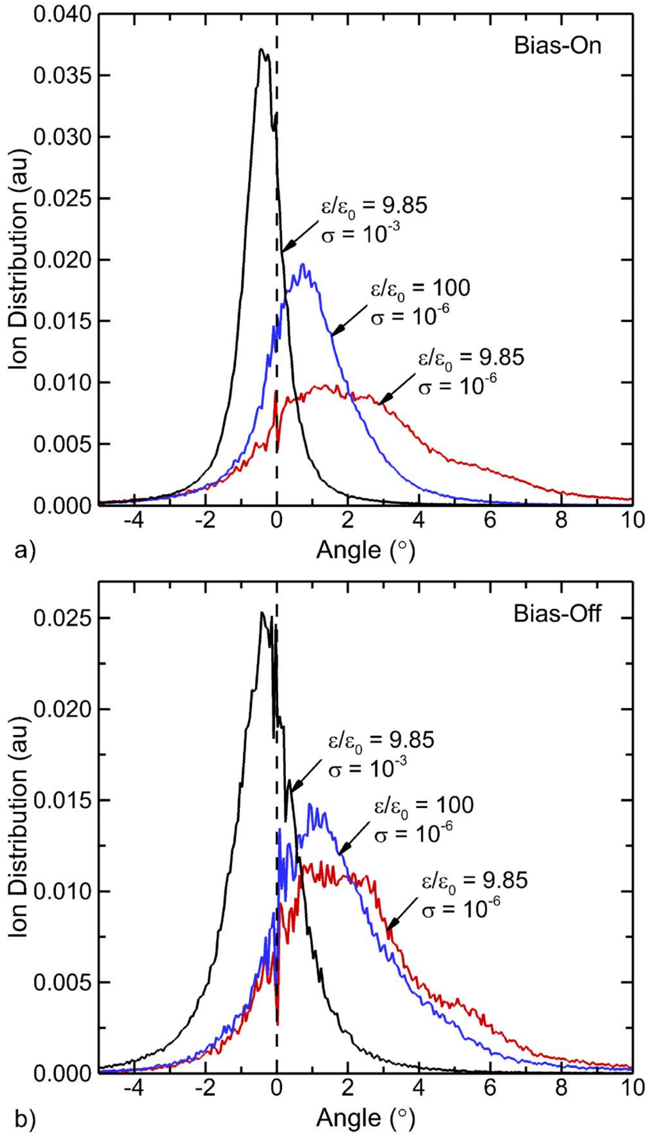

FIG. 17. Ion angular distributions at the edge of the wafer for focus ring permittivities and conductivities of 9.85 and 10^{-6} S/cm, 100 and 10^{-6} S/cm, and 9.85 and 10^{-3} S/cm averaged over (a) bias-on and (b) bias-off portions of the pulsed period.

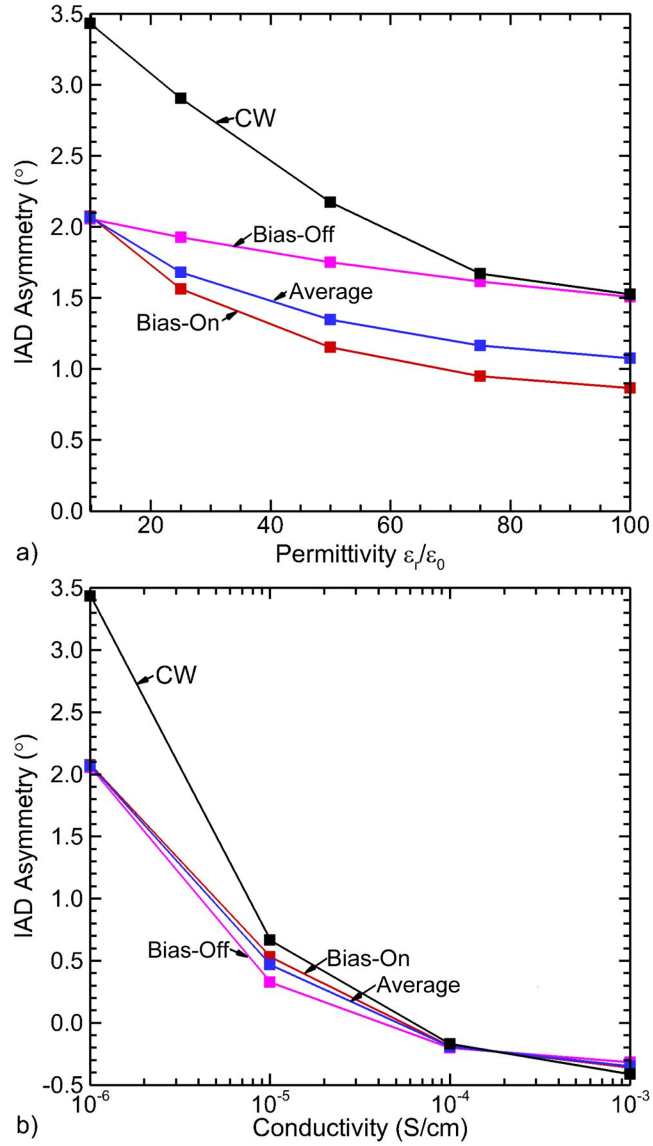

FIG. 18. Deviation of the ion angular distribution from the normal at the edge of wafer for focus ring (a) relative permittivities of 9.85–100 and (b) conductivities of 10^{-6}–10^{-3} S/cm. The RF bias is 250 kHz and is pulsed with a 50% DC and 10 kHz PRF.

With, on average, a smaller sheath potential during the bias-off period, there is less opportunity for the electric field in the sheath to reorient to the vertical ion trajectories that enter the sheath with non-normal velocities.

The angular tilt in the IEAD at the edge of the wafer is shown in Fig. 18 as a function of FR permittivity and conductivity for otherwise the base case for pulsing. Comparisons are made to CW results. The tilt in the IAD generally decreases with increasing permittivity of the FR as there is less charging of the FR with the higher capacitance. With less charging, there is more voltage available for the sheath over the FR, producing a sheath whose thickness is more commensurate with that over the wafer. The result is less curvature to the sheath and less tilt to the IAD. In spite of there being only nominal changes to the IED during pulsing when varying permittivity of the FR, there is a significant reduction to the tilt of the IAD at the edge of the wafer and particularly so with respect to CW results. The growth and shrinkage of the sheath over the FR during pulsing produce, on average, less curvature at the edge of the wafer. The reduction in tilt of the IAD is less during the bias-off period relative to CW than during the bias-on period. The FR more fully discharges during the pulse-off period when the current collected by the FR consists largely of conduction current.

When increasing the conductivity of the FR from 10^{-6} to 10^{-3} S/cm, the pulse average ion angular asymmetry changes the direction from pointing inward at low conductivity to pointing outward at large conductivity as mentioned before. With increasing conductivity, less voltage is dropped across the FR (which now resembles a leaky capacitor). The voltage division between the FR and the sheath then applies the majority of the voltage to the sheath. Although the higher conductivity FR acts as an extension of the powered electrode, the voltage division between the wafer and the sheath above the wafer provides less voltage to the sheath compared to the sheath over the FR and so has a thinner sheath. As a result, the curvature of the sheath reverses, producing an outward-directed tilt. At lower FR conductivities, the tilt (both positive and negative) is less severe when pulsing.

VI. CONCLUDING REMARKS

Customizing ion energy distributions to wafers in plasma processing is a continuing challenge. Pulsing the bias serves many purposes in process development, one being the opportunity to control or influence the IEAD. A computational investigation was performed on the influence of pulsing a low frequency (250 kHz) bias applied to the substrate in an ICP. The plasma was sustained in an $Ar/Cl_2/O_2$ mixture at 15 mTorr, for PRF of the bias of 2–50 kHz, DC of 10%–90%, blocking capacitance (C_B) of 100–1000 nF, FR relative permittivities of 9.85–100, and FR conductivities of 10^{-6}–10^{-3} S/cm. These conditions were chosen to produce RC time constants, τ_C, for charging and discharging C_B to be commensurate with the pulse period.

If τ_C is short compared to the pulse period, then the bias-on and bias-off periods are fairly independent. The bias-on period has a well-defined and nearly constant V_{DC}, whereas during the bias-off phase, V_{DC} will dissipate resulting in a low-energy ion flux to the wafer. For combinations of PRF and DC producing bias-on and bias-off periods that are commensurate to τ_C, V_{DC} will be dynamic during the pulse period. For our conditions, V_{DC} increases to more negative values during bias-on and less negative values during bias-off. The end result is a broadening or narrowing of the range of energy of the IEAD delivered to the substrate.

This modification of the IEAD is less significant during the bias-on period as the IEAD is dominated by the oscillation of the bias voltage, whose amplitude will always be larger than the magnitude of V_{DC}. The peak-maximum energy (the most probable energy which ions strike the wafer) during the bias-on period is most sensitive to conditions in which V_{DC} is most dynamic. The major influence on the IEAD due to dynamics in V_{DC} is during the bias-off when the RF bias is not active. Here, the applied voltage generating the sheath is the decaying V_{DC}, which produces IEADs having a narrower energy spread. The energy width of the IEAD is then a function of the time rate of change of V_{DC}, which, in turn, is inversely proportional to τ_C.

Alterations to the electrical properties of the FR surrounding the powered electrode impact the conduction and displacement current flowing to the blocking capacitor, which then influences the dynamics of V_{DC} during the pulse period. Increasing the permittivity of the FR increases its capacitance, increasing the displacement current to the blocking capacitor through the FR. However, this displacement current contributes a small fraction of the total current responsible for charging and discharging C_B. As a consequence, the periodic dynamics in V_{DC} are not hugely sensitive to the permittivity of the FR. Significant changes to the dynamics of V_{DC} occur when the conductivity of the FR is increased, which enables conduction current to flow through FR to C_B.

Although not a major focus of this investigation, the angular tilt of ions incident onto the edge of the wafer can be influenced by the PRF, DC, τ_C, and properties of the FR. This influence is manifested through the relative changes in sheath thickness over the FR compared to over the wafer, as these relative thicknesses determine sheath curvature at the edge of the wafer. We found that the tilt to the IAD to the edge of the wafer is typically less severe when pulsing compared to CW operation. With CW excitation, particularly at low frequency, the FR fully charges during the RF cycle, which thins the sheath above the FR producing sheath curvature. With pulsing the sheath thickness over the FR is, on average, more commensurate with that over the wafer, producing less sheath curvature.

ACKNOWLEDGMENT

This work was supported by Samsung Electronics Co.

AUTHOR DECLARATIONS

Conflict of Interest

The authors have no conflicts to disclose.

Author Contributions

Evan Litch: Conceptualization (equal); Data curation (lead); Formal analysis (lead); Investigation (lead); Methodology (lead); Software (lead); Visualization (lead); Writing – original draft (lead); Writing – review & editing (equal). **Hyunjae Lee:** Conceptualization (equal); Funding acquisition (equal); Project administration (equal); Supervision (supporting); Writing – review & editing (supporting). **Sang Ki Nam:** Conceptualization (equal); Funding acquisition (equal); Supervision (supporting); Writing – review & editing (supporting). **Mark J. Kushner:** Conceptualization (equal); Funding acquisition (equal); Investigation (equal); Project administration (lead); Software (supporting); Supervision (lead); Writing – review & editing (equal).

DATA AVAILABILITY

The data that support the findings of this study are available within the paper and from the corresponding authors upon reasonable request.

REFERENCES

[1]R. R.C, M. Sangli, S. Sripad, N. R, L. N, and E. D, Analog Integr. Circuits Signal Process. **125**, 22 (2025).
[2]G. S. Oehrlein *et al.*, J. Vac. Sci. Technol. B **42**, 041501 (2024).
[3]M. Shen *et al.*, Jpn. J. Appl. Phys. **62**, SI0801 (2023).
[4]C.-F. Han, C.-C. Lin, and J.-F. Lin, Precis. Eng. **71**, 141 (2021).
[5]E. G. Shustin, J. Commun. Technol. Electron. **62**, 454 (2017).
[6]B. R. Rogers and T. S. Cale, Vacuum **65**, 267 (2002).
[7]G.-R. Lee, S.-W. Hwang, J.-H. Min, and S. H. Moon, J. Vac. Sci. Technol. A **20**, 1808 (2002).
[8]J.-H. Min, G.-R. Lee, J. Lee, S. H. Moon, and C.-K. Kim, J. Vac. Sci. Technol. B **22**, 893 (2004).
[9]E. Kawamura, V. Vahedi, M. A. Lieberman, and C. K. Birdsall, Plasma Sources Sci. Technol. **8**, R45 (1999).
[10]E. Litch, H. Lee, S. K. Nam, and M. J. Kushner, J. Vac. Sci. Technol. A **43**, 033001 (2025).
[11]Y. Zhang, J. Liu, Y. Liu, and X. Wang, Phys. Plasmas **11**, 3840 (2004).
[12]M. A. Sobolewski, J. K. Olthoff, and Y. Wang, J. Appl. Phys. **85**, 3966 (1999).
[13]D. J. Economou, J. Phys. D: Appl. Phys. **47**, 303001 (2014).
[14]S. Banna *et al.*, IEEE Trans. Plasma Sci. **37**, 1730 (2009).
[15]A. Agarwal, P. J. Stout, S. Banna, S. Rauf, K. Tokashiki, J.-Y. Lee, and K. Collins, J. Appl. Phys. **106**, 103305 (2009).
[16]J. W. Coburn and H. F. Winters, Appl. Phys. Lett. **55**, 2730 (1989).
[17]D. Hoffman, V. Godyak, J. G. Yang, and S. Shannon, "IEEE Conference Record—Abstracts," in *2005 IEEE International Conference on Plasma Science*, Monterey, CA, 20–23 June 2005 (IEEE, Piscataway, NJ, 2005), p. 107.
[18]M. J. Kushner, J. Phys. D: Appl. Phys. **42**, 194013 (2009).
[19]F. Krüger, H. Lee, S. K. Nam, and M. J. Kushner, J. Vac. Sci. Technol. A **41**, 013006 (2023).
[20]P. Tian and M. J. Kushner, Plasma Sources Sci. Technol. **26**, 024005 (2017).
[21]S. Huang, V. Volynets, J. R. Hamilton, S. Lee, I.-C. Song, S. Lu, J. Tennyson, and M. J. Kushner, J. Vac. Sci. Technol. A **35**, 031302 (2017).
[22]S. Tinck, W. Boullart, and A. Bogaerts, Plasma Sources Sci. Technol. **20**, 045012 (2011).
[23]J.-H. Kim, Y.-H. Shin, and K.-H. Chung, Thin Solid Films **435**, 288 (2003).
[24]M. A. Lieberman and A. J. Lichtenberg, *Principles of Plasma Discharges and Materials Processing* (Wiley, New York, 2005).
[25]B. G. Heil, U. Czarnetzki, R. P. Brinkmann, and T. Mussenbrock, J. Phys. D: Appl. Phys. **41**, 165202 (2008).
[26]U. Czarnetzki, J. Schulze, E. Schüngel, and Z. Donkó, Plasma Sources Sci. Technol. **20**, 024010 (2011).
[27]T. Lafleur, Plasma Sources Sci. Technol. **25**, 013001 (2016).
[28]D. Levko, R. R. Upadhyay, K. Suzuki, and L. L. Raja, J. Vac. Sci. Technol. B **41**, 012205 (2023).
[29]D. Kim and D. J. Economou, J. Appl. Phys. **95**, 3311 (2004).
[30]E. V. Barnat and G. A. Hebner, Appl. Phys. Lett. **85**, 3393 (2004).